Sustainable Energy & Fuels

Probing the Origins of Photodegradation in Organic-Inorganic Metal Halide Perovskites with Time-Resolved Mass Spectrometry

Journal:	*Sustainable Energy & Fuels*
Manuscript ID	SE-ART-07-2018-000358.R1
Article Type:	Paper
Date Submitted by the Author:	07-Aug-2018
Complete List of Authors:	Song, Zhaoning; University of Toledo, Physics and Astronomy Wang, Changlei; University of Toledo, Department of Physics and Astronomy Phillips, Adam; The University of Toledo, Physics and Astronomy Grice, Corey; The University of Toledo, Physics and Astronomy Zhao, Dewei; University of Toledo, Physics and Astronomy Yu, Yue; the university of toledo, Chen, Cong; The University of Toledo, Physics and Astronomy Li, Chongwen; The University of Toledo, Physics and Astronomy Yin, Xingxin; The University of Toledo, Physics and Astronomy Ellingson, Randy; University of Toledo, Physics and Astronomy Heben, Michael; University of Toledo Yan, Yanfa; University of Toledo, Department of Physics and Astronomy

SCHOLARONE™
Manuscripts

Probing the Origins of Photodegradation in Organic-Inorganic Metal Halide Perovskites with Time-Resolved Mass Spectrometry

Zhaoning Song, Changlei Wang, Adam B. Phillips, Corey R. Grice, Dewei Zhao, Yue Yu, Cong Chen, Chongwen Li, Xinxing Yin, Randy J. Ellingson, Michael J. Heben and Yanfa Yan

University of Toledo, Wright Center for Photovoltaics Innovation and Commercialization, Department of Physics and Astronomy, 2801 W. Bancroft St., Toledo, OH, 43606 USA.

Corresponding Author
*E-mail: yanfa.yan@utoledo.edu

Abstract

Operational and long-term stability of perovskite solar cells are critical for their commercialization at large scale. To mitigate the stability issues, the fundamental understanding of physicochemical processes associated with the degradation of perovskite materials is needed. Here, we measure time resolved mass spectrometry of the evolved gas species during the photoinduced degradation of organic-inorganic lead trihalide perovskites with commonly-used monovalent cations, including methylammonium (MA), formamidinium (FA), and Cs. Our results indicate that the hot-carrier-induced deprotonation of MA^+ cations is the fundamental origin of the photodegradation, which inevitably leads to the release of volatile species such as ammonium (NH_3), aminocarbyne fragments (CNH_2), hydrogen (H_2), and iodine/hydrogen iodide (I/HI) from methylammonium lead iodide ($MAPbI_3$) at different rates under simulated one sun solar illumination. The photodegradation processes can be mitigated by applying ultra-violet (UV) filters with proper cutoff wavelengths to the light source. Additionally, we demonstrate that the incorporation of FA reduces the release of organic species but does not prevent the formation of I/HI. However, the addition of Cs effectively suppresses the release of all volatile gases. The best photostability is obtained from the FA/Cs mixed perovskites, showing that the complete removal of MA from mixed-cation perovskite is preferred for more photostable perovskites.

Introduction

In the past few years, organic-inorganic metal halide perovskites have emerged as an exciting class of photovoltaic (PV) materials.[1, 2] With high certificated power conversion efficiencies that exceed 23.3%[3] and low-cost solution-based fabrication processes, perovskite solar cells (PVSCs) are projected to rival other more established PV technologies in the market, especially on the aspects of the levelized costs of energy (LCOE),[4] life-cycle environmental impacts,[5, 6] and energy payback time (EPBT).[7, 8] Recent progress on large-area deposition techniques,[9-11] combining with advances in materials engineering to improve device performance and durability,[12-17] makes PVSCs attractive for more practical, commercial applications. However, major obstacles remain before high volume deployment of perovskite PV modules becomes feasible.[18] The most critical one is the lack of operational and long-term stability. To be commercially viable, PVSCs need to retain robust stability throughout their lifetimes. The fact that most established PV companies provide a 25-year warranty for their products sets a high bar for perovskite PV technology to enter the energy production market.[19]

Over the last decade, lifetimes of PVSCs reported in literature have extended from few hours to over a year.[20] However, most high efficiency perovskite solar cells based on triple-cation (methylammonium, MA; formamidinium, FA; Cs) lead trihalide perovskites exhibit a certain degree of degradation under continuous operational conditions.[21] In an attempt to understand and eliminate degradation, the origins and processes of the device degradation are under intense investigation.[22] Degradation mechanisms of metal halide perovskite materials and devices under different environmental conditions have been extensively explored.[23-35] In general, a variety of extrinsic factors, including light,[36-42] heat,[43-45] atmosphere (e.g., oxygen and moisture),[42, 46-48] and electric filed,[49, 50] are attributed to the degradation of perovskite materials and devices. Among

them, heat, moisture, and electric filed related degradation can be mitigated by employing appropriate encapsulation and interface protection,[16, 51-53] while solar irradiation that contains substantial energetic photons is an unavoidable stress during the operation of a solar cell.

A recent literature review that surveyed 50 publications shows that the stability of PVSCs is strongly reduced under illumination,[36] which hinders the practical application of PVSCs. To mitigate this photoinstability issue, the fundamental understanding of physicochemical processes associated with the photodegradation of perovskite materials is needed. Thus far, only a few studies have investigated the degradation processes of perovskite films under illumination via X-ray photoelectron, diffraction, and absorption spectroscopies,[40-42] with an emphasis on monitoring the chemical and structural changes in the perovskite films. Despite these efforts, little is known about the formation and escape rates of the volatile decomposition products during the photodegradation processes. Most recently, Nickel et al. reported an investigation on the photodegradation of $MAPbI_3$ by analyzing the residual gas composition,[39] providing insights on understanding the photodegradation mechanisms, However, the measurements of gas effusion were limited to few selected low atomic weight (< 32) gas molecules, and volatile species across the full spectrum of the photodegradation products, especially iodine or iodide vapors, are not yet unraveled. The missing information may hinder the accurate understanding of the degradation mechanism and underestimate the impact of MA on the stability of state-of-the-art triple-cation (FA/MA/Cs) perovskites, which have demonstrated much improved photostability than mixed FA/MA perovskites.[13, 14, 54] Therefore, more detailed work is needed to develop a comprehensive understanding of the underlying degradation mechanisms and pathways.[55]

Herein, we address this need, by employing high-resolution time resolved mass spectrometry (MS) to monitor the gas emission during the photodegradation of organic-inorganic halide

perovskites in vacuum and under different illumination conditions. Starting with the archetypal perovskite, methylammonium lead iodide ($CH_3NH_3PbI_3$ or $MAPbI_3$), we measure the escape rates of volatile photodecomposition products and identify the photon energy threshold for the photodegradation of $MAPbI_3$ using a filtered light source. For the first time, we observed that MA gas is released faster than HI under illumination, indicating that photodegradation is likely originated from the hot carrier-induced deprotonation of MA^+ cations. Moreover, we study the photostability of a series of FA/MA/Cs mixed-cation perovskites, demonstrating that the incorporation of FA does not fully stop the photodegradation, but the incorporation of nonvolatile Cs^+ into perovskite films leads to improved photostability. The results show that the complete removal of MA from mixed-cation perovskites is preferred for more photostable perovskites.

Results and Discussion

We start our investigation with the archetypal perovskite material, i.e., $MAPbI_3$. A built-in-house temperature programmed deposition spectroscopy system[56] (Figure S1) was used to measure *in-situ* evolution of MS, and to identify the chemical compositions of the released gases from $MAPbI_3$ under simulated solar radiation. Figure 1a shows the evolution of mass-to-charge ratio (m/z) spectrum recorded as a function of light exposure time (See the Experimental Methods for details). A variety of gas species including H_2 (m/z = 2), NH_3 (m/z = 17), H_2O (m/z =18), CH_3NH_2 (m/z = 28 - 31), HI (m/z = 64 or 128), and I_2 (m/z = 127) were detected. By measuring these partial pressures as a function of time, the photodegradation dynamics of $MAPbI_3$ was determined (vide infra). The comparison of the relevant peaks at the initial stage and at a time during the photodegradation are shown in Figure 1b-f. The significant increase in the partial pressures of the gas signals clearly indicates the presence of the volatile decomposition products

through photodecomposition of $MAPbI_3$. It is worth noting that MS signals are comprised of the fragments of molecules due to the electron bombardment during the ionization process in the quadrupole ion analyzer. Multiple fragments from a gas content can be detected, and one fragment species may originate from different parent molecules. Because of this, the chemical compositions that revealed by MS are manifold, and chemical complexity needs considered while analyzing the data.

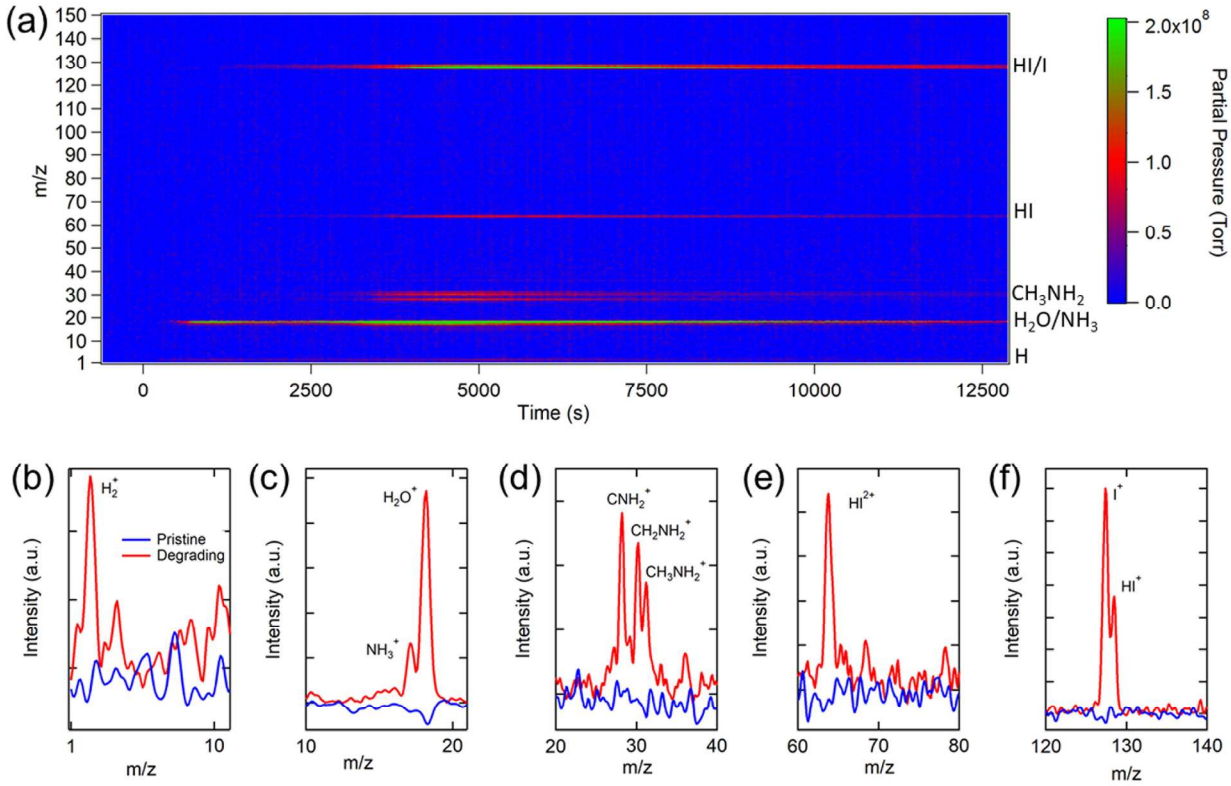

Figure 1. (a) Evolution of mass spectrum (m/z) of the released gases during the photoinduced decomposition of $CH_3NH_3PbI_3$. Comparison of the characteristic m/z peaks of the pristine and degrading sample, including (b) H^+, (c) NH_3^+/H_2O^+, (d) CNH_2^+/ $CH_2NH_2^+$/ $CH_3NH_2^+$, (e) HI^{2+}, and (f) I^+/HI^+.

Turning to the detailed analysis of photodegradation process, the release of H_2O was initiated after the $MAPbI_3$ was exposed to light for ~ 5 min (300 s). Due to the hygroscopic nature of perovskites,[46] water molecules could either be adsorbed on the surface of the perovskite[57] or infiltrate in grain boundaries to form the hydrated perovskite phases.[58] The observation of photo-induced desorption of water indicates the high physisorption affinity of water molecules to perovskites, which leads to substantial water adsorption even for a short time exposure (2 to 3 min) to the air during the sample transfer. However, the amount of water desorbed from perovskite is challenging to quantify because water contributes significantly to the base pressure of a typical high vacuum (~10^{-7} Torr) chamber (Figure S2), and its partial pressure is sensitive to the subtle chamber condition changes and degassing of other gas species. Therefore, water is not used as the primary indicator for the photodegradation analysis in this study.

The release of methylamine (CH_3NH_2 or MA) and HI signals commenced at ~20 min (1200 s), signifying the beginning of photodegradation of $MAPbI_3$. The peaks observed at m/z = 2 (Figure 1b) and m/z = 17 and 18 (Figure 1c), corresponding to H_2 and NH_3/H_2O, respectively, could be directly produced by the photodecomposition of $MAPbI_3$ or from the ionization byproducts of MA. The released MA was characterized by three aminocarbyne fragments at m/z ratios of 28 (CNH_2), 30 (CH_2NH_2), and 31(CH_3NH_2), as shown in Figure 1d, which is consistent with the reference MS of MA (Figure S3). The release of NH_3 and MA gas molecules can break the phase equilibrium homogeneity in $MAPbI_3$ and worsen the decomposition of pristine perovskite phase by triggering a phase transfer from the pure corner-sharing Pb-I octahedra perovskite network into an inhomogeneous combination of $MAPbI_3$ perovskite, layered PbI_2, and the low-

dimensional perovskites.[59, 60] This phase transition creates more vulnerable defect sites on the grain boundaries with loose bonding or dangling bonds that are prone to decomposition.

The release of HI gas was evident in the single and double charged HI with m/z ratios of 128 and 64, respectively (Figure 1e and f), which was not found in the previous photodegradation study.[39] The signal of m/z = 127 could be attributed to HI as well as the single charged I or double charged I_2, indicating an equilibrium between I_2 and I^- exists in the perovskite films during photodegradation. The condensation of I_2 residues on the inner wall of the sample conditioning tube (Figure S4) reveals the simultaneous formation of I_2 gas with HI, consistent with a recent report on measuring optical absorption spectrum of I_2 release from $MAPbI_3$ in toluene under illumination.[61] Both I_2 and HI are detrimental to the stability of perovskite films. Iodine vapor could induce severe degradation of $MAPbI_3$ due to chemical chain reactions.[62] HI is a high corrosive acid which could cause severe damage to the perovskite crystals upon contact and accelerate the degradation of perovskites.

The aforementioned results reveal that the MA derivatives and I_2/HI gases are the primary volatile products during the photodegradation of $MAPbI_3$. Interestingly, the photodegradation products of $MAPbI_3$ differ from thermal degradation in which CH_3I and NH_3 were detected at above 300 ˚C by MS measuremensts.[44] Although photo- and thermal degradation results in different products, there should be a chemical equilibrium between these gasses, which favors the formation of MA and HI at low temperatures (~60 ˚C under illumination) but tends to form CH_3I and NH_3 at high temperatures (> 300 ˚C). Nonetheless, for both degradation pathways, the decomposition of perovskite is associated with the release of volatile gases, especially MA and HI. It is noteworthy that while some work has demonstrated that photo-induced superoxide formed in presence of oxygen or oxide interface leads to the photodecomposition of

perovskite,[37, 63-65] the results here show that oxygen is not necessary for the photodecomposition since no oxygen or superoxide signals were detected.

To further elucidate the degradation mechanisms, we measured the photon energy dependences of the photodegradation of $MAPbI_3$. Long pass filters with various cutoff wavelengths were used to remove the high energy photons that are known to be particularly detrimental to PVSCs.[39, 64] Figure 2 show the evolution of the MS traces of MA and HI from $MAPbI_3$ films exposed to illumination with the spectra filtered with short wavelength photons being cut off at 280, 320, 370, 395, 420, and 455 nm. The transmittance spectra of the filters and full spectra of the MS data are shown in Figure S5 and S6, respectively.

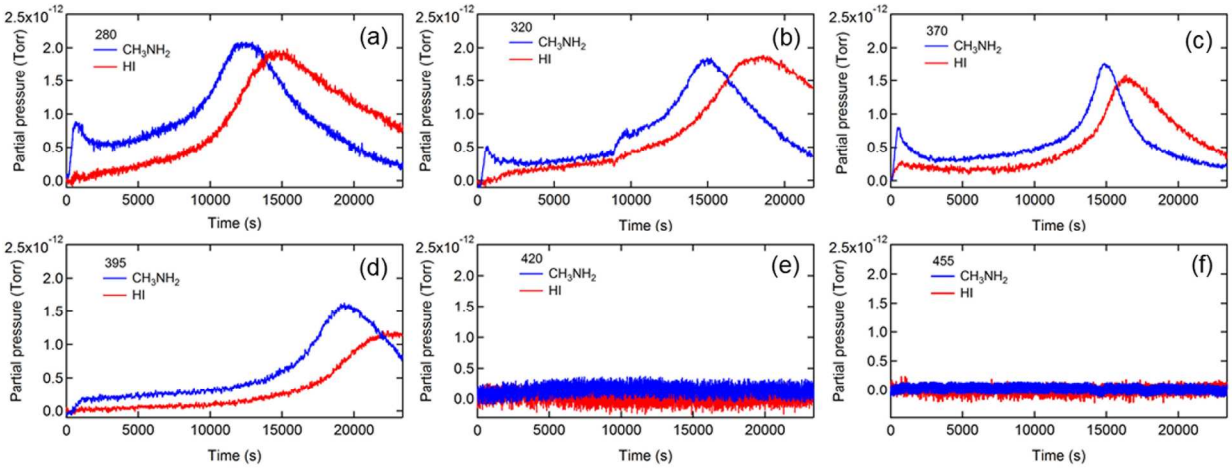

Figure 2. Mass spectroscopy traces of CH_3NH_2 (28-31) and HI (126-127) during the photodecomposition of $MAPbI_3$ films under the illumination of a xenon lamp equipped with a long pass optical filter with a cutoff wavelength of (a) 280, (b) 320, (c) 370, (d) 395, (e) 420, and (f) 455 nm.

Insights into the dynamics and kinetics of photodegradation of $MAPbI_3$ can be obtained from analyzing the gas emission processes. First, the MS traces of MA and HI (Figure 2a-d) show a general trend of an increase in MA and HI partial pressures to the maxima followed by a decline to a residual level, indicating the photodegradation of $MAPbI_3$ is a self-limiting process that likely initiates on the surface of the film or at grain boundaries, reaches the pressure maxima when most surface bonds are cleaved, and then slows down due to the formation of more photostable PbI_2 on the surface. This finding is consistent with the report that photodegradation of $MAPbI_3$ saturated after the decomposition of the surface layer.[38] Beyond that, the escape rates of the residual gas determined by the time derivative of the partial pressure decreased with increasing the cutoff wavelength (Figure S7), likely due to the retarded photodegradation by removing highly energetic photons. The residual gas signals were in the minimum detectable range and negligible when the 420 (Figure 2e) and 455 nm (Figure 2f) filters were applied, respectively, indicating a minimum photon energy of 2.95 eV (~420 nm) is needed for triggering light-induced degradation of $MAPbI_3$. Considering the bandgap of 1.55 eV for $MAPbI_3$,[45] the excess kinetic energy of photoexcited charge carriers (~1.4 eV) is close to the energy associated with the deprotonation of MA^+ cations (1.49 eV) reported in the literature.[66] It is worth noting that our result is more accurate than the minimum energy of 2.72 eV required for the light-induced dissociation of $MAPbI_3$ perovskite reported by Nickel et al.[39] To verify that the mitigation of photodecomposition is merely due to removal of high energy photons rather than reduction of light intensity, we performed the MS measurements under reduced illumination intensities (25%) achieved by using neutral density filter with ODs of 0.6. Figure S8 shows evidence of photodecomposition even under this weak illumination condition (~25 mW/cm^2), confirming the high energy photons are responsible for photodegradation of $MAPbI_3$.

The detailed analysis of *in-situ* MS measurement data provides insights into the kinetics of the photodecomposition process. Interestingly, MA exhibits higher partial pressure than HI at the early stage of photodecomposition process and reach the peak prior to HI in most cases (Figure 2a-d), indicating that MA is released faster than HI when photodegradation occurs. The result reveals that MA^+, i.e., $CH_3NH_3^+$ (the protonation of MA molecule), is more vulnerable against high energy photons than I^- and is more likely to be the origin of photodegradation of perovskite. It is worth noting that a clear initial spike in the MA signal was observed in some $MAPbI_3$ films (Figure 2a-c), likely due to the existence of MA^+ cations on film surfaces and in grain boundaries.[67] It is known that $MAPbI_3$ surfaces contain under coordinated MA^+ cations.[68] Photoexcitation could release those loosely bounded MA gas molecules by a deprotonation process, leading to the initial spike in the MA signal.

Applying a filter to eliminate UV photons is an effective strategy to improve the photostability of perovskite materials and devices. Additionally, when the perovskite films are fully encapsulated, the volatile photodecomposition products cannot escape and thus persist in the films, retaining the perovskite phase. However, these approaches do not solve the intrinsic instability issue of $MAPbI_3$. Alternatively, many studies suggest that incorporation of less volatile large organic (e.g., formamidinium (FA)) and monovalent metal cations (e.g., Cs^+) can significantly enhance photostability.[1, 14, 69] To explore the effect of the A-site cation on the photostability of perovskite materials, we performed MS measurements on a variety of single- and mixed cation perovskites. Figure 3a shows the accumulated MS signals of organic species (i.e. MA and FA derivatives) and HI for perovskite films with various $(Cs_xFA_yMA_{1-x-y})PbI_3$ compositions, including $MAPbI_3$, $FAPbI_3$, $MA_{0.7}FA_{0.3}PbI_3$, $FA_{0.95}Cs_{0.05}PbI_3$, $FA_{0.9}Cs_{0.1}PbI_3$, $FA_{0.8}Cs_{0.2}PbI_3$, and $(MA_{0.7}FA_{0.3})_{0.8}Cs_{0.2}PbI_3$, after 7 h light exposure. Detailed traces of the corresponding curves are

shown in Figure S9. As expected, we found $MAPbI_3$ had the most severe photodecomposition. Interestingly, gravimetric analysis shows that $MAPbI_3$ lost about ~30% of initial weight, more than the weight ratio (25.6%) of MAI (159 g/mol) to $MAPbI_3$ (620 g/mol), indicating the further decomposition of PbI_2 into metallic lead (Pb^0) and I_2 gas.[41, 70] $FAPbI_3$ show significantly lower emission of organic species (mainly in terms of CNH and CNH_2) but comparable HI compared with $MAPbI_3$ (Figure 3b). Although improved photostability of $FAPbI_3$ was reported,[69] the significant release of HI could still fundamentally limit the durability of $FAPbI_3$. In contrast, incorporating Cs into $FAPbI_3$ significantly suppressed the photodecomposition of perovskite materials. The photostability of perovskite increases with increasing Cs proportion, with $FA_{0.8}Cs_{0.2}PbI_3$ showing the two orders of magnitude less materials loss during continuous illumination (Figure 3c). Interestingly, the addition of MA to the mixed-cation perovskites (FA/MA and FA/MA/Cs) shows worse photostability than their pure FA and FA/Cs counterparts, indicating the UV-photons induced degradation of the perovskites is mainly attributed to MA cations.

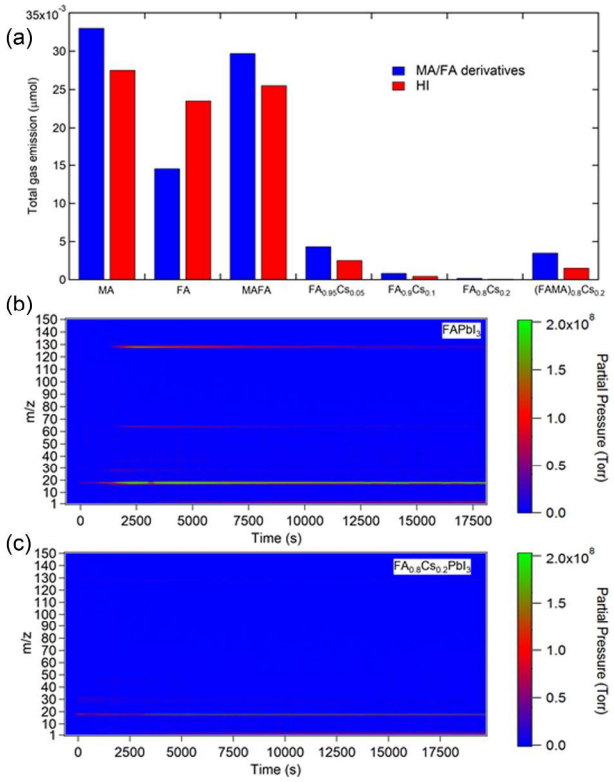

Figure 3. Total amounts of organic species and HI gases released from various perovskite films, including $MAPbI_3$, $FAPbI_3$, $MA_{0.7}FA_{0.3}PbI_3$, $FA_{0.95}Cs_{0.05}PbI_3$, $FA_{0.9}Cs_{0.1}PbI_3$, $FA_{0.8}Cs_{0.2}PbI_3$, and $(MA_{0.7}FA_{0.3})_{0.8}Cs_{0.2}PbI_3$ under the simulated illumination of 100 mW/cm^2 for 7 h. Time-resolved mass spectra of (b) $FAPbI_3$ and (c) $FA_{0.8}Cs_{0.2}PbI_3$ under the simulated illumination of 100 mW/cm^2.

The above observation leads us to hypothesize that the photodegradation mechanism of MA-contained perovskites proceeds through a sequence of steps involving: (1) photoexcitation of hot carriers; (2) deprotonation of MA cations and formation of MA gas near surface or grain boundary regions; and (3) formation of HI gas and iodine vacancies (V_I) (deterioration of PbI_6 octahedron), as described by Equation (1) - (3) and shown in Figure 4.

$$h\nu\ (> 3\ eV)\ \rightarrow e^{-}\ (hot) + h^{+}(hot) \quad (1)$$

$$CH_3NH_3{}^{+}\ + e^{-}\ (hot)\ \rightarrow CH_3NH_2\ (g) + H^{+} + e^{-} \quad (2)$$

$$H^{+}\ + I^{-}\ \rightarrow\ HI\ (g) + V_I \quad (3)$$

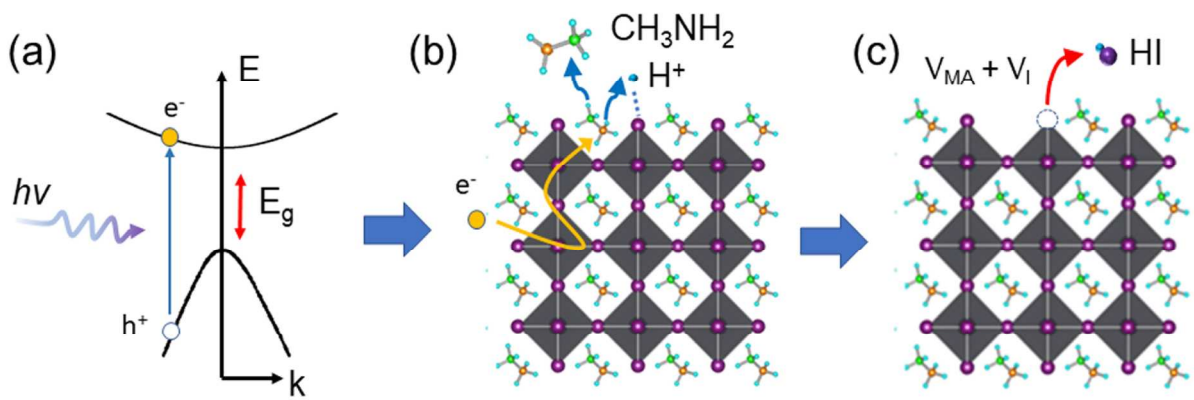

Figure 4. Schematic representation of photodegradation mechanism. (a) Hot carrier generation, (b) deprotonation and release of MA gas, and (c) formation of HI gas and V_I.

The generation of long lived hot electrons is a requisite for the observed photodegradation of $MAPbI_3$ (Equation (1) and Figure 4a). Recent studies reported that hot carriers in perovskite have a relatively long lifetime (~100 ps) and can migrate a long distance (up to 600 nm) in perovskite crystals.[71-73] A hot electron may interact with a MA cation via columbic coupling. The hot electron may transfer its excess energy to the MA cation and deprotonate it, releasing free protons and volatile MA gas (Equation (2) and Figure 4b). The free protons then pair with under coordinated I atoms on the surface, forming HI gas and iodine vacancies (i.e., deteriorated PbI_6 octahedra) (Equation (3) and Figure 4c). We speculate that HI formation is the most detrimental species to the stability of perovskite because the continuous loss of HI can cause the breakdown

of the Pb-I framework via an equilibrium phase transfer from the corner-shared to the face shared Pb-I octahedra, leading to the catastrophic decomposition of $MAPbI_3$ into PbI_2. The loss of HI completely changes the morphology of $MAPbI_3$ films, turning the compact and smooth perovskite films into discrete PbI_2 crystals (Figure S10). Although the primary gas products of the photodegradation are MA and HI, other gas species, such as H_2, NH_3, and I_2, may coexist via a photochemical equilibrium in the atmosphere. Nonetheless, preventing the formation of volatile gases could be an effective strategy to mitigate the photoinstability issue of perovskite.

The mechanism of improved stability of Cs contained perovskite is attributed to the low volatility of Cs. Due to its small ionic size (167 pm) compared with MA^+ (217 pm) and FA^+ (253 pm),[74] it is reasonable to expect Cs^+ ions to segregate into surface and grain boundaries, a process that reduces strain and, therefore, is energetically favorable. As discussed earlier, organic MA and FA cations tend to deprotonate and vaporize after receiving energy from hot carriers generated by high energetic photons. In contrast, Cs has much lower vapor pressures and has no proton. Preserving monovalent cations limits the formation and release of HI gas, locking iodine atoms in the perovskite framework. Therefore, the intrinsic decomposition of iodine-based perovskites can be eliminated, showing the potential for long-term stability. However, the triple cation $(MA_{0.7}FA_{0.3})_{0.8}Cs_{0.2}PbI_3$, unlike its FA/Cs counterpart, still released substantial amounts of organic species and HI gases under continuous illumination (Figure 3), indicating the intrinsic instability of perovskite materials incorporating MA cations. To overcome the instability issue, the MA contents in the perovskites should be reduced or eliminated.

Conclusion

In summary, we have investigated the photodecomposition of $MAPbI_3$ under different illumination conditions using MS. We demonstrated that photodecomposition is a self-limited process, identified the photon energy threshold of ~ 3 eV to trigger the decomposition of $MAPbI_3$, and showed that the release of MA is prior to HI. Lastly, we found that incorporating Cs and removing MA can improve photostability of perovskite materials. Our findings suggest that compositional engineering of perovskite materials and UV filtering can prevent the photodegradation of the organic components and thus increase the operational and long-term stability of organic-inorganic halide perovskite solar cells.

Experimental

Synthesis of perovskite thin films

The perovskite films were synthesized following a previously published method. Details are included in the Supplemental Information.

Time-resolved mass spectroscopy measurements

Mass spectra of perovskite films were obtained using a custom dynamically-pumped temperature programmed desorption system. For each degradation measurement, a perovskite film (1 inch by 0.25 inch) was placed in a quartz tube that connected to the primary chamber of the system. The system was pumped down for ~20 h to allow degassing of the specimen prior to the photon induced degradation measurement. The chamber was evacuated to $<10^{-7}$ Torr before each measurement. The degradation process was monitored using a quadrupole mass spectrometer (Stanford Research System, RGA 300). The mass spectrum with a range of 1 to 150 atomic mass

unit (AMU) was recorded in a 5 s interval. Prior to the illumination, background signals were first collected for 10 min in dark and the averages were subtracted from the main signals. After that, the sample was exposed to a simulated solar irradiance of ~100 mW/cm^2 generated by a Xenon arc lamp. For the spectroscopic-dependent measurements, a long wavelength filters with the cutoff edge at 280, 320, 370, 395, 420, or 455 nm were used to eliminate the influence of high energy photons.

Conflicts of interest

The authors declare no competing financial interest.

Acknowledgements

This work is financially supported by the Office of Naval Research under Contract no. N00014-17-1-2223, the Air Force Research Laboratory, Space Vehicles Directorate (contract # FA9453-11-C-0253), the National Science Foundation under contract no. CHE−1230246 and DMR−1534686, the U.S. Department of Energy (DOE) SunShot Initiative under the Next Generation Photovoltaics 3 program (DE-FOA-0000990), and the Ohio Research Scholar Program.

Author contribution

Z. S. and Y.F.Y. conceived the project. Z. S. carried out the MS measurements. C. W., Y. Y., C. C., X. Y. and C. L. synthesized perovskite thin films and helped characterization. C. R. G., A. B. P. and M. J. H. assisted the MS measurements. Z. S. and Y. F. Y. analyzed the data and wrote the manuscript. D. Z., A. B. P., R. J. E. and M. J. H. helped with the manuscript preparation. All the authors discussed the results and commented on the manuscript. Y.F.Y. supervised the project.

References

1. J.-P. Correa-Baena, M. Saliba, T. Buonassisi, M. Grätzel, A. Abate, W. Tress and A. Hagfeldt, *Science*, 2017, **358**, 739-744.
2. J. J. Berry, J. van de Lagemaat, M. M. Al-Jassim, S. Kurtz, Y. Yan and K. Zhu, *ACS Energy Lett.*, 2017, **2**, 2540-2544.
3. NREL, Solar Cell Efficiency Chart, https://www.nrel.gov/pv/assets/images/efficiency-chart-20180716.jpg, (accessed 6 August 2018).
4. Z. Song, C. L. McElvany, A. B. Phillips, I. Celik, P. W. Krantz, S. C. Watthage, G. K. Liyanage, D. Apul and M. J. Heben, *Energy Environ. Sci.*, 2017, **10**, 1297-1305.
5. J. Gong, S. B. Darling and F. You, *Energy Environ. Sci.*, 2015, **8**, 1953-1968.
6. I. Celik, Z. Song, A. J. Cimaroli, Y. Yan, M. J. Heben and D. Apul, *Sol. Energy Mater. Sol. Cells*, 2016, **156**, 157-169.
7. I. Celik, A. B. Phillips, Z. Song, Y. Yan, R. J. Ellingson, M. J. Heben and D. Apul, *Energy Environ. Sci.*, 2017, **10**, 1874-1884.
8. I. Celik, A. B. Phillips, Z. Song, Y. Yan, R. J. Ellingson, M. J. Heben and D. Apul, *IEEE J. Photovol.*, 2017, **8**, 305-309.
9. Z. Li, T. R. Klein, D. H. Kim, M. Yang, J. J. Berry, M. F. A. M. van Hest and K. Zhu, *Nat. Rev. Mater.*, 2018, **3**, 18017.
10. H. Chen, F. Ye, W. Tang, J. He, M. Yin, Y. Wang, F. Xie, E. Bi, X. Yang, M. Grätzel and L. Han, *Nature*, 2017, **550**, 92.
11. M. Yang, Z. Li, M. O. Reese, O. G. Reid, D. H. Kim, S. Siol, T. R. Klein, Y. Yan, J. J. Berry, M. F. A. M. van Hest and K. Zhu, *Nat. Energy*, 2017, **2**, 17038.
12. M. Saliba, T. Matsui, K. Domanski, J.-Y. Seo, A. Ummadisingu, S. M. Zakeeruddin, J.-P. Correa-Baena, W. R. Tress, A. Abate, A. Hagfeldt and M. Grätzel, *Science*, 2016, **354**, 206-209.
13. M. Saliba, T. Matsui, J.-Y. Seo, K. Domanski, J.-P. Correa-Baena, M. K. Nazeeruddin, S. M. Zakeeruddin, W. Tress, A. Abate, A. Hagfeldt and M. Gratzel, *Energy Environ. Sci.*, 2016, **9**, 1989-1997.
14. H. Tsai, R. Asadpour, J.-C. Blancon, C. C. Stoumpos, O. Durand, J. W. Strzalka, B. Chen, R. Verduzco, P. M. Ajayan, S. Tretiak, J. Even, M. A. Alam, M. G. Kanatzidis, W. Nie and A. D. Mohite, *Science*, 2018, **360**, 67-70.
15. W. S. Yang, B.-W. Park, E. H. Jung, N. J. Jeon, Y. C. Kim, D. U. Lee, S. S. Shin, J. Seo, E. K. Kim, J. H. Noh and S. I. Seok, *Science*, 2017, **356**, 1376-1379.
16. J. A. Christians, P. Schulz, J. S. Tinkham, T. H. Schloemer, S. P. Harvey, B. J. Tremolet de Villers, A. Sellinger, J. J. Berry and J. M. Luther, *Nat. Energy*, 2018, **3**, 68-74.
17. M. Abdi-Jalebi, Z. Andaji-Garmaroudi, S. Cacovich, C. Stavrakas, B. Philippe, J. M. Richter, M. Alsari, E. P. Booker, E. M. Hutter, A. J. Pearson, S. Lilliu, T. J. Savenije, H. Rensmo, G. Divitini, C. Ducati, R. H. Friend and S. D. Stranks, *Nature*, 2018, **555**, 497.
18. A. Abate, J. P. Correa‐Baena, M. Saliba, M. S. Su'ait and F. Bella, *Chem. - Eur. J.*, 2018, **24**, 3083-3100.
19. M. A. Green, *Nat. Energy*, 2016, **1**, 15015.

20. G. Grancini, C. Roldán-Carmona, I. Zimmermann, E. Mosconi, X. Lee, D. Martineau, S. Narbey, F. Oswald, F. De Angelis, M. Graetzel and M. K. Nazeeruddin, *Nat. Commun.*, 2017, **8**, 15684.
21. K. Domanski, E. A. Alharbi, A. Hagfeldt, M. Grätzel and W. Tress, *Nat. Energy*, 2018, **3**, 61-67.
22. T. Leijtens, G. E. Eperon, N. K. Noel, S. N. Habisreutinger, A. Petrozza and H. J. Snaith, *Adv. Energy Mater.*, 2015, **5**, 1500963.
23. D. Wang, M. Wright, N. K. Elumalai and A. Uddin, *Sol. Energy Mater. Sol. Cells*, 2016, **147**, 255-275.
24. M. I. Asghar, J. Zhang, H. Wang and P. D. Lund, *Renewable Sustainable Energy Rev.*, 2017, **77**, 131-146.
25. X. Guo, C. McCleese, C. Kolodziej, A. C. S. Samia, Y. Zhao and C. Burda, *Dalton Trans.*, 2016, **45**, 3806-3813.
26. Y. Yao, G. Wang, F. Wu, D. Liu, C. Lin, X. Rao, R. Wu, G. Zhou and Q. Song, *RSC Adv.*, 2017, **7**, 42973-42978.
27. Z. Li, C. Xiao, Y. Yang, S. P. Harvey, D. H. Kim, J. A. Christians, M. Yang, P. Schulz, S. U. Nanayakkara, C.-S. Jiang, J. M. Luther, J. J. Berry, M. C. Beard, M. M. Al-Jassim and K. Zhu, *Energy Environ. Sci.*, 2017, **10**, 1234-1242.
28. K. Domanski, B. Roose, T. Matsui, M. Saliba, S.-H. Turren-Cruz, J.-P. Correa-Baena, C. R. Carmona, G. Richardson, J. M. Foster, F. De Angelis, J. M. Ball, A. Petrozza, N. Mine, M. K. Nazeeruddin, W. Tress, M. Gratzel, U. Steiner, A. Hagfeldt and A. Abate, *Energy Environ. Sci.*, 2017, **10**, 604-613.
29. Z. Song, J. Werner, S. C. Watthage, F. Sahli, N. Shrestha, S. D. Wolf, B. Niesen, A. B. Phillips, C. Ballif, R. J. Ellingson and M. J. Heben, *IEEE J. Photovol.*, 2017, **7**, 1563-1568.
30. N. H. Tiep, Z. Ku and H. J. Fan, *Adv. Energy Mater.*, 2016, **6**, 1501420.
31. E. Smecca, Y. Numata, I. Deretzis, G. Pellegrino, S. Boninelli, T. Miyasaka, A. La Magna and A. Alberti, *Phys. Chem. Chem. Phys.*, 2016, **18**, 13413-13422.
32. A. Gomez, S. Sanchez, M. Campoy-Quiles and A. Abate, *Nano Energy*, 2018, **45**, 94-100.
33. Natalia N. Shlenskaya, N. A. Belich, M. Grätzel, E. A. Goodilin and A. B. Tarasov, *J. Mater. Chem. A*, 2018, **6**, 1780-1786.
34. F. U. Kosasih and C. Ducati, *Nano Energy*, 2018, **47**, 243-256.
35. Y.-H. Kye, C.-J. Yu, U.-G. Jong, Y. Chen and A. Walsh, *J. Phys. Chem. Lett.*, 2018, **9**, 2196-2201.
36. F. Lang, O. Shargaieva, V. V. Brus, H. C. Neitzert, J. Rappich and N. H. Nickel, *Adv. Mater.*, 2018, **30**, 1702905.
37. D. Bryant, N. Aristidou, S. Pont, I. Sanchez-Molina, T. Chotchunangatchaval, S. Wheeler, J. R. Durrant and S. A. Haque, *Energy Environ. Sci.*, 2016, **9**, 1655-1660.
38. Y. Li, X. Xu, C. Wang, B. Ecker, J. Yang, J. Huang and Y. Gao, *J. Mater. Chem. C*, 2017, **121**, 3904-3910.
39. N. H. Nickel, F. Lang, V. V. Brus, O. Shargaieva and J. Rappich, *Adv. Electron. Mater.*, 2017, **3**, 1700158.
40. R.-P. Xu, Y.-Q. Li, T.-Y. Jin, Y.-Q. Liu, Q.-Y. Bao, C. O'Carroll and J.-X. Tang, *ACS Appl. Mater. Interfaces*, 2018, **10**, 6737-6746.

41. X. Tang, M. Brandl, B. May, I. Levchuk, Y. Hou, M. Richter, H. Chen, S. Chen, S. Kahmann, A. Osvet, F. Maier, H.-P. Steinruck, R. Hock, G. J. Matt and C. J. Brabec, *J. Mater. Chem. A*, 2016, **4**, 15896-15903.
42. B.-A. Chen, J.-T. Lin, N.-T. Suen, C.-W. Tsao, T.-C. Chu, Y.-Y. Hsu, T.-S. Chan, Y.-T. Chan, J.-S. Yang, C.-W. Chiu and H. M. Chen, *ACS Energy Lett.*, 2017, **2**, 342-348.
43. B. Conings, J. Drijkoningen, N. Gauquelin, A. Babayigit, J. D'Haen, L. D'Olieslaeger, A. Ethirajan, J. Verbeeck, J. Manca, E. Mosconi, F. D. Angelis and H.-G. Boyen, *Adv. Energy Mater.*, 2015, **5**, 1500477.
44. E. J. Juarez-Perez, Z. Hawash, S. R. Raga, L. K. Ono and Y. Qi, *Energy Environ. Sci.*, 2016, **9**, 3406-3410.
45. Z. Song, S. C. Watthage, A. B. Phillips, B. L. Tompkins, R. J. Ellingson and M. J. Heben, *Chem. Mater.*, 2015, **27**, 4612-4619.
46. A. M. A. Leguy, Y. Hu, M. Campoy-Quiles, M. I. Alonso, O. J. Weber, P. Azarhoosh, M. van Schilfgaarde, M. T. Weller, T. Bein, J. Nelson, P. Docampo and P. R. F. Barnes, *Chem. Mater.*, 2015, **27**, 3397-3407.
47. A. J. Pearson, G. E. Eperon, P. E. Hopkinson, S. N. Habisreutinger, J. T.-W. Wang, H. J. Snaith and N. C. Greenham, *Adv. Energy Mater.*, 2016, **6**, 1600014.
48. Z. Song, A. Abate, S. C. Watthage, G. K. Liyanage, A. B. Phillips, U. Steiner, M. Graetzel and M. J. Heben, *Adv. Energy Mater.*, 2016, **6**, 1600846.
49. T. Leijtens, E. T. Hoke, G. Grancini, D. J. Slotcavage, G. E. Eperon, J. M. Ball, M. De Bastiani, A. R. Bowring, N. Martino, K. Wojciechowski, M. D. McGehee, H. J. Snaith and A. Petrozza, *Adv. Energy Mater.*, 2015, **5**, 1500962.
50. Y. Yuan, Q. Wang, Y. Shao, H. Lu, T. Li, A. Gruverman and J. Huang, *Adv. Energy Mater.*, 2016, **6**, 1501803.
51. F. Bella, G. Griffini, J.-P. Correa-Baena, G. Saracco, M. Grätzel, A. Hagfeldt, S. Turri and C. Gerbaldi, *Science*, 2016, **354**, 203-206.
52. F. Matteocci, L. Cinà, E. Lamanna, S. Cacovich, G. Divitini, P. A. Midgley, C. Ducati and A. Di Carlo, *Nano Energy*, 2016, **30**, 162-172.
53. R. Cheacharoen, N. Rolston, D. Harwood, K. A. Bush, R. H. Dauskardt and M. D. McGehee, *Energy Environ. Sci.*, 2018, **11**, 144-150.
54. C. Wang, Z. Song, Y. Yu, D. Zhao, R. A. Awni, C. R. Grice, N. Shrestha, R. J. Ellingson, X. Zhao and Y. Yan, *Sustainable Energy & Fuels*, 2018, DOI: 10.1039/C8SE00200B.
55. J. A. McLeod and L. Liu, *J. Phys. Chem. Lett.*, 2018, **9**, 2411-2417.
56. K. E. Hurst, M. J. Heben, J. L. Blackburn, T. Gennett, A. C. Dillon and P. A. Parilla, *Rev. Sci. Instrum.*, 2013, **84**, 025103.
57. R. Long, W. Fang and O. V. Prezhdo, *J. Phys. Chem. Lett.*, 2016, **7**, 3215-3222.
58. Q. Wang, B. Chen, Y. Liu, Y. Deng, Y. Bai, Q. Dong and J. Huang, *Energy Environ. Sci.*, 2017, **10**, 516-522.
59. Y. Zhao and K. Zhu, *Chemical Communications*, 2014, **50**, 1605-1607.
60. C. Li, S. Pang, H. Xu and G. Cui, *Solar RRL*, 2017, **1**, 1700076.
61. G. Y. Kim, A. Senocrate, T.-Y. Yang, G. Gregori, M. Grätzel and J. Maier, *Nat. Mater.*, 2018, **17**, 445-449.
62. S. Wang, Y. Jiang, Emilio J. Juarez-Perez, Luis K. Ono and Y. Qi, *Nat. Energy*, 2016, **2**, 16195.
63. N. Aristidou, C. Eames, I. Sanchez-Molina, X. Bu, J. Kosco, M. S. Islam and S. A. Haque, *Nat. Commun.*, 2017, **8**, 15218.

64. T. Leijtens, G. E. Eperon, S. Pathak, A. Abate, M. M. Lee and H. J. Snaith, *Nat. Commun.*, 2013, **4**, 3885.
65. Q. Sun, P. Fassl, D. Becker‐Koch, A. Bausch, B. Rivkin, S. Bai, P. E. Hopkinson, H. J. Snaith and Y. Vaynzof, *Adv. Energy Mater.*, 2017, **7**, 1700977.
66. E. L. Øiestad, Å. M. L. Øiestad, H. Skaane, K. Ruud, T. Helgaker, E. Uggerud and T. Vulpius, *Eur. Mass Spectrom.*, 1995, **1**, 121-129.
67. D. W. deQuilettes, W. Zhang, V. M. Burlakov, D. J. Graham, T. Leijtens, A. Osherov, V. Bulović, H. J. Snaith, D. S. Ginger and S. D. Stranks, *Nat. Commun.*, 2016, **7**, 11683.
68. J. Haruyama, K. Sodeyama, L. Han and Y. Tateyama, *J. Am. Chem. Soc.*, 2015, **137**, 10048-10051.
69. J.-W. Lee, D.-J. Seol, A.-N. Cho and N.-G. Park, *Adv. Mater.*, 2014, **26**, 4991-4998.
70. J. Schoonman, *Chemical Physics Letters*, 2015, **619**, 193-195.
71. Z. Guo, Y. Wan, M. Yang, J. Snaider, K. Zhu and L. Huang, *Science*, 2017, **356**, 59-62.
72. J. Huang, Y. Yuan, Y. Shao and Y. Yan, *Nat. Rev. Mater.*, 2017, **2**, 17042.
73. S. A. Bretschneider, F. Laquai and M. Bonn, *J. Mater. Chem. C*, 2017, **121**, 11201-11206.
74. G. Han, H. D. Hadi, A. Bruno, S. A. Kulkarni, T. M. Koh, L. H. Wong, C. Soci, N. Mathews, S. Zhang and S. G. Mhaisalkar, *J. Mater. Chem. C*, 2018, **122**, 13884-13893.

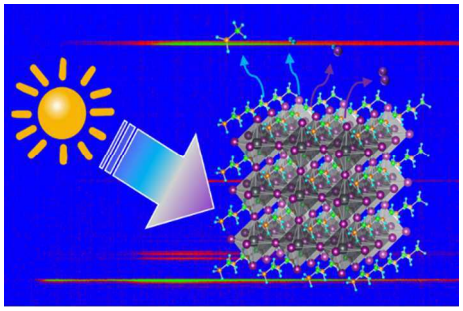

Our mass spectrometry measurements indicate that the hot-carrier-induced deprotonation of MA^+ cations is the fundamental origin of the photodegradation.